THE JOURNAL OF PHYSICAL CHEMISTRY C

Article

pubs.acs.org/JPCC

A Computational Study of Semiconducting Benzobisthiazoles: Analysis of the Substituent Effects on the Electronic Structure, Solid-State Interactions, and Charge Transport Properties Using DFT Methods

N. L. Janaki, B. Priyanka, Anup Thomas, and K. Bhanuprakash*

Inorganic and Physical Chemistry Division, Indian Institute of Chemical Technology, Hyderabad 500 607, India

Supporting Information

ABSTRACT: In this study, using DFT methods, we analyze the electronic structures at both the molecular and solid-state level of the recently suggested three-dimensional semiconducting bis(hexylthieno)benzobisthiazole molecule (**2**), the unsubstituted benzobisthiazole ring (**1**), its 2,6-disubstituted derivatives (**3** and **4**), and its 2,6-dihexyl-4,8-dithiophene derivative (**7**). The uniqueness of **2**, as per literature reports, is the close intermolecular contacts in the three directions (3D ordering) due to the crystal packing which should lead to more efficient charge transport. Gas-phase geometry optimization of the above molecules using the B3LYP functional is carried out and compared with the X-ray data. Reorganization energies to estimate the charge transfer, calculated using the same functional, do not indicate any particular bias toward hole transport or electron transport process. Transfer integrals (for estimation of intermolecular charge hopping pathways) between the HOMOs (for hole transport) are quite large in the $\pi-\pi$ stacked direction in the **1**−**3** crystals, while in n-type **4** the transfer integrals between the LUMOs are large. In the case of **7**, which has not been tested so far for its semiconducting properties, the calculated transfer integral is very small and reorganization energies are large, indicating that it may show poorer performance when compared to the other derivatives. Analysis of the intermolecular interactions (noncovalent) in the crystals has been carried out using dispersion-corrected functionals, namely B2PLYP-D, M06-2X, and B97-D. For the 2,6 derivatives, a maximum of ∼24 kcal/mol interaction energy (B2PLYP-D) is obtained in the $\pi-\pi$ stacking direction but for the S−N contacts the binding energies are only around 5−6 kcal/mol. In **7**, the binding energies obtained are much smaller and in the range of 2−9 kcal/mol only. Band structure calculations using the PBE functional of crystal **2** are also carried out. We conclude from this study that this fused heterocyclic ring at the molecular level by itself is not in the same class like semiconducting pentacene or rubrene but substituted benzobisthiazole rings pack in the crystal in some cases like **2**, **3**, and **4** to yield very large transfer integrals which can play a crucial role in charge transport. The present work will be helpful to understand and rationally design molecules which self-assemble in the solid state giving intermolecular close contacts in the crystal.

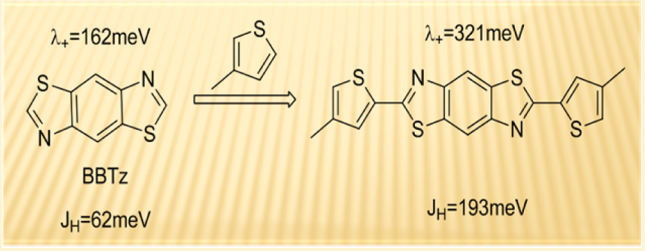

INTRODUCTION

Organic π-conjugated materials with semiconducting properties are of immense research interest because of their potential applications as active elements in organic light-emitting devices (OLED), organic field effect transistors (OFET), organic thin film transistors (OTFT), and photovoltaic cells.[1−9] These materials offer certain advantages over the standard/existing inorganic materials like versatility of chemical synthesis, low cost, ease of fabrication, molding into thin films, and the tuning of properties through suitable substitution.[10,11] The search for new and efficient charge transport material remains as one of the most active areas in this field.[12−18] While bringing out efficient devices is one challenge, understanding the interactions, properties due to substitutions, geometry, and packing of the molecules in the solid state is another.[19−22] The optoelectronic applicability of such materials depends on various factors such as appropriate HOMO and LUMO energy levels, easiness for the mobility of hole and electron, and the geometrical packing in the solid state.[19] The charge-transfer processes are very much influenced by the geometry and molecular packing as well as by the intermolecular interaction parameters.[19] Thus, it follows that a proper understanding of all these molecular characteristics of the organic materials used in organic semiconductor devices is an important prerequisite for the design and selection of appropriate molecules as well as for optimizing the performance of the devices. Here, quantum chemical studies of these molecular properties have proven to be invaluable and have been shown to be of immense help in designing and improving the devices.[20−25]

Received: May 21, 2012
Revised: September 13, 2012
Published: October 10, 2012

Scheme 1. Molecular Structures and Bond Numbering Scheme Discussed in This Work

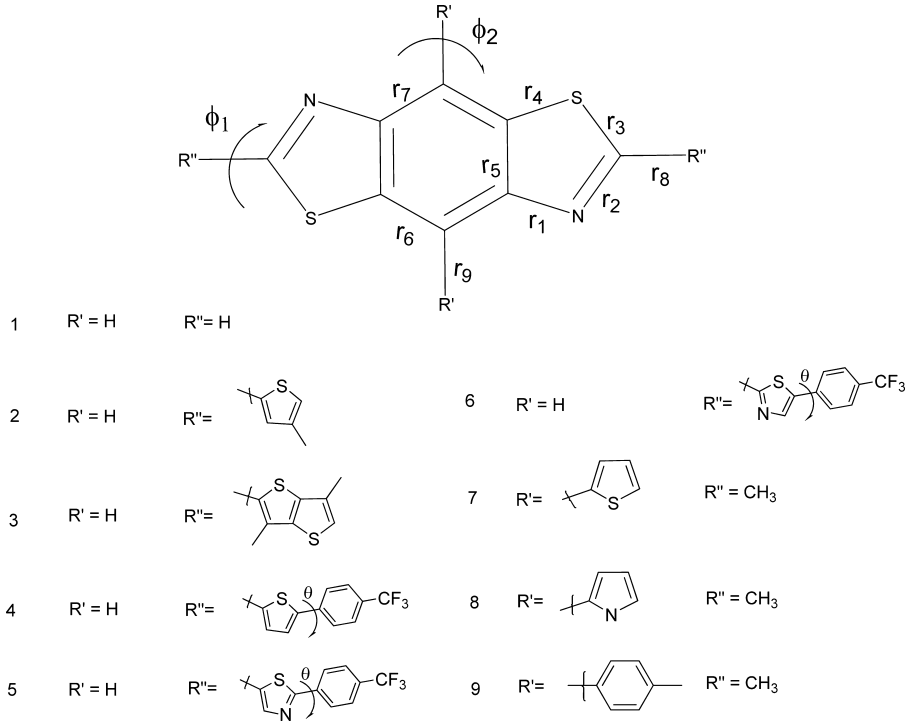

A very common design strategy is to introduce electron-rich donors (D) or electron-deficient acceptors (A) to a suitable core structure to achieve p-type (hole transport) and n-type (electron transport) semiconductors, respectively.[26,27] Or, in other words, molecules with high electron affinity (EA) and low ionization potentials (IP) with favorable intermolecular interactions would be suitable as n-type and p-type semiconductors, respectively. Ambipolar charge carrier transport is also achieved by appending both D and A functionality to the same core structure. A number of organic semiconducting materials have been designed and used in OLED's and OFET's which have shown promising performance.[12,28] Compared to p-type materials, fewer n-type materials have been reported.[29] Ambipolar materials are rarer.[30,31]

Recently, fused heteroaromatic rings have emerged as promising candidates for organic semiconductor technology.[32−38] This is due to the fact that the fused structures lead to stabilized HOMOs and a wide HOMO−LUMO gap (HLG) and a favorable intermolecular $\pi-\pi$ overlap, which are necessary for performance of the device.[36] One such example is benzo(1,2-*d*:4,5-*d*′)bisthiazole (**1**) derivatives (Scheme 1) showing semiconducting properties which have been reported recently.[34−37] The central benzobisthiazole ring (BBTz) is an electron-deficient nitrogen heterocyclic system (benzene is fused in between two electron-withdrawing thiazole rings) with high electron affinity which enhances the air stability in p-type conductors and increases the easiness of electron injection in the n-type semiconductors.[34] It has advantages of planar structure which can lead to a better interchain $\pi-\pi$ self-assembly.[35,36] In addition, it offers functionalization or substitution that can be done either at the 2,6-position or/and at the 4,8-position. The 2,6-substituted BBTz (**2**−**6**) are the only ones experimentally characterized for FET performance, while only photophysical properties are known for the 4,8-substituted ones (**7**−**9**).[38] Recently, Skabara and co-workers synthesized alkyl-substituted thiophene and thienothiophene as donors at the 2,6-position of the BBTz ring derivatives (**2** and **3**).[35,36] The hole mobilities obtained are in the order of 10^{-2} and 10^{-3} cm^2 V^{-1} s^{-1}, respectively. More interestingly, the monomers self-assemble to a 3D network with very close intermolecular noncovalent contacts.[35] In **2**, each orthogonal molecule is involved in intermolecular S−N contacts between thiazole rings in one dimension along with inter ring $\pi-\pi$ contacts of 3.50 and 3.56 Å in the other two dimensions, which is claimed to be a unique collection of 3D close contacts.[35] Mamada et al. have synthesized BBTz derivatives (**4**−**6**) for n-type semiconduction with electron-withdrawing substituents at the 2,6-position and achieved a good electron-transfer mobility of about 0.24 cm^2 V^{-1} s^{-1} for one of the molecules, **4**.[37]

Though experimental studies have been reported for these molecules, there is no theoretical characterization that can provide us the causes or origin for the hole mobility in **2** and **3** and electron mobility in **4, 5**, and **6**. A detailed theoretical analysis would also provide us an understanding of the 3D nature of charge transfer as inferred from experiments for **2**.[35] Hence, a systematic investigation of donor/acceptor derivatives of these BBTz molecules, which are promising semiconductor materials, is carried out in this work. Here we have chosen for this study three of the BBTZ derivatives, namely p- type **2** and **3** and n-type **4** for which both crystal structures and mobility studies are available. We have also chosen **1**, which is the bare moiety and for which only the crystal structure is available, for comparison. In addition, we also investigate crystal **7**, the 4,8-disubstituted BBTz molecule for which no semiconduction experimental data has been reported to the best of our knowledge. We carry out the geometry optimization of the neutral molecules, and their cations and anions, which leads to the information on their molecular geometries, and HOMO and LUMO energy levels. Calculations of reorganization energies to estimate the hole and electron transport properties in these molecules are also carried out. From the crystal structure, the intermolecular interaction energies and the transfer integrals for both hole and electron mobilities are also estimated for all possible dimer interaction pathways. The

dx.doi.org/10.1021/jp304892x | *J. Phys. Chem. C* 2012, 116, 22663−22674

band structure for the crystal **2** is also generated to get a good insight into the dispersion. This detailed study presented here should be helpful in understanding and designing more efficient BBTz derivatives for semiconduction.

COMPUTATIONAL METHODS

We have carried out the geometry optimization of the molecules **1**, **2**, **3**, **4**, and **7** (scheme 1) using the Gaussian 09 software.[39] For computational simplicity, hexyl chains, where present, are replaced by methyl groups. This replacement is not expected to change the results and the trends. Minimization is carried out at the DFT-B3LYP level using the Berny optimization algorithm with a default integration grid and 6-311G(d,p) basis sets for all the atoms except for the sulfur atom where additional 3f and 3d functions have been added, i.e., 6-311G(3df,3pd). The additional basis set on S atom results in better representation of the C−S bond. The B3LYP functional consists of Becke's three-parameter hybrid exchange functional combined with the Lee−Yang−Parr correlation functional.[40−42] Frequency calculations are carried out to ensure that each optimized conformation has all positive frequencies and thus is a minimum on the potential energy surface. The atomic positions of the molecules in all possible geometrical conformations were fully relaxed and only the low-lying minima are reported.

To assess the charge carrier injection easiness, we also estimated HOMO, LUMO eigenvalues, the ionization potential (IP), and electron affinity (EA) by taking the energy differences between the ground and ionized states (nonrelaxed ionized state gives vertical IP/EA and relaxed ionized state gives adiabatic IP/EA) (ΔSCF method).[43]

Two widely used theories for describing the charge mobilities in organic materials are the band theory[44,45] and the hopping model.[46,47] With the overlap of neighboring molecules' MOs, the band is formed through which the conduction of the charge takes place according to the band theory model. On the other hand, the hopping model is more suitable where coupling between neighboring molecules is small (as in the case here). Using this model, the charge transport that is calculated is the intermolecular process in which the charge hops between two molecules. The hole and electron transport process at the molecular level in the charge carrier transporting layers can then be portrayed as the electron-transfer/hole-transfer reactions between the neighboring molecules.

$$A^{+/\cdot} + A' \rightarrow A' + A^{+/\cdot}$$

where A′ is the neutral molecule interacting with neighboring oxidized or reduced $A^{+/-}$. In the case of electron transport, the interaction can be considered between a molecule in the neutral state interacting with a radical anion and in the case of hole transport the interaction can be considered between a molecule in the neutral state and a radical cation. The rate constant for charge transfer (CT) can be defined using the Marcus theory[48]

$$k_{ct} = 4pJ^2/h(1/4p\lambda k_b T)^{1/2} \exp(-\lambda/4k_b T)$$

where J is the transfer integral/coupling matrix element (J_H for hole and J_L for electron) between neighboring molecules, λ is the reorganization energy (λ_+ for hole and λ_- for electron), k_b is the Boltzmann constant, and T is the temperature.

The contribution of the environmental factor (intermolecular) to the reorganization energy due to the neighboring molecules is expected to be small in organic solids and hence only the intramolecular reorganization energy is calculated.[23] The intramolecular reorganization energies is the sum of stabilization gained by relaxation of the neutral molecule after losing/gaining electron and stabilization gained by charged species after gaining/losing electron. The quantum mechanical evaluation of $\lambda_\pm$ requires the awareness of the potential energy profile of the cation and anion.[23] So we have carried out the optimization of the cation and anion at the UB3LYP level for all the molecules in this study.

The reorganization energies are calculated based on the model shown in Scheme 2. This model has been applied with success in many earlier studies.[22−25,49] Here, the energy required (λ_1) in electronvolts for the reorganization of the neutral geometry to the cation geometry upon removal of an electron and the energy required (λ_2) to reorganize the obtained cation geometry back to a neutral state upon reaccepting an electron added up give the total reorganization energy (λ_+) of the molecule when the charge is being transported. In a similar fashion the reorganization energy (λ_-) of the neutral to anion (λ_3) and back (λ_4) should be useful in understanding the electron transport.

Scheme 2. Calculation of the Reorganization Energy

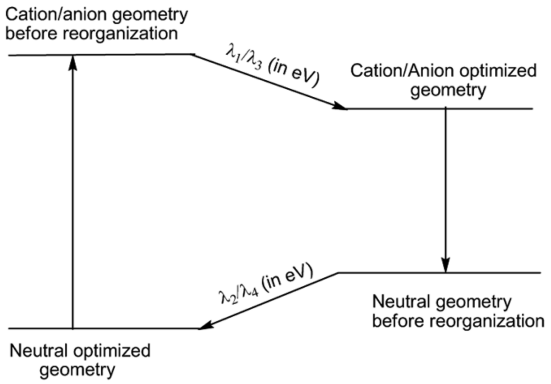

$\lambda_+ = \lambda_1 + \lambda_2$ λ_+ (for Hole Transport)

$\lambda_- = \lambda_3 + \lambda_4$ λ_- (for Electron Transport)

The reorganization energies are also calculated on the basis of normal-mode analyses of isolated molecules. In this calculation scheme the total reorganization energies can be partitioned into individual contribution from each vibrational mode.[50] Normal-mode analyses were performed using DUSHIN program by postprocessing the frequency analysis results from Gaussian 09. In the harmonic approach the relaxation energy is[23]

$$\lambda = \sum \lambda_i = \sum \hbar\omega S_i$$

$$\lambda_i = \frac{k_i}{2}\Delta Q_i^{\,2}, \quad S_i = \frac{\lambda_i}{\hbar\omega_i}$$

In the above equation, k_i and ΔQ_i represent force constant and displacement along normal mode Q_i between the equilibrium geometries of neutral and charged molecules. ω_i represents the vibrational frequencies and S_i denotes the Huang−Rhys factor (vibrational coupling constant for hole/electron).

The charge-transfer integral is estimated for all the possible dimer interaction pathways by taking pairs of molecule in the crystal, using the recently suggested entire dimer Hamiltonian (EDH) method by Siebbles and co-workers[51] and J. L. Bredas and co-workers,[52] by orthogonalization of off-diagonal elements of Kohn−Sham Hamiltonian as shown in the following equation.

dx.doi.org/10.1021/jp304892x | J. Phys. Chem. C 2012, 116, 22663−22674

Table 1. Comparison of Optimized Geometries of 1−4 and 7 with Crystal Geometries[a]

bonds	1	2[b]	3	4	7
r_1(C−N)	1.386 (1.397)	1.377 (1.391/1.379)	1.373 (1.407)	1.376 (1.391)	1.382 (1.393)
r_2(C−N)	1.289 (1.286)	1.298 (1.292/1.317)	1.303 (1.320)	1.3 (1.305)	1.290 (1.304)
r_3(C−S)	1.754 (1.740)	1.775 (1.786/1.766)	1.779 (1.775)	1.774 (1.747)	1.760 (1.744)
r_4(C−S)	1.742 (1.734)	1.743 (1.709/1.753)	1.742 (1.730)	1.742 (1.730)	1.747 (1.749)
r_5(C−C)	1.426 (1.420)	1.426 (1.441/1.435)	1.426 (1.415)	1.427 (1.424)	1.422 (1.410)
r_6(C−C)	1.388 (1.385)	1.387 (1.387/1.379)	1.387 (1.393)	1.386 (1.383)	1.404 (1.397)
r_7(C−C)	1.396 (1.395)	1.398 (1.370/1.409)	1.399 (1.380)	1.398 (1.397)	1.412 (1.419)
r_8(C−C)	–	1.446 (1.444/1.453)	1.444 (1.445)	1.444 (1.443)	1.496 (1.505)
r_9(C−C)	–	–	–	–	1.466 (1.469)
ϕ_1	–	–	–	–	33.50 (21.42)
ϕ_2	–	0.0 (0.84/0.676)	0.0 (3.02)	1.02 (1.93)	–
θ	–	–	–	26.1 (5.54)	–

[a]Experimental values (Å) given in parentheses.[34−38] [b]This crystal has two orthogonal half-units A and B in the asymmetric unit which differ in geometry; experimental values are given in the order (A/B). Computed values are obtained using B3LYP/6-311G(d,p) for C, N, H, and F and 6-311G(3df,3pd) for S.

$$H = \begin{bmatrix} \langle \varphi_1|\mathrm{H}|\varphi_1\rangle & \langle \varphi_1|\mathrm{H}|\varphi_2\rangle \\ \langle \varphi_2|\mathrm{H}|\varphi_1\rangle & \langle \varphi_2|\mathrm{H}|\varphi_2\rangle \end{bmatrix}$$

where φ_1 and φ_2 are the localized monomer orbitals.

This mainly requires the knowledge of the dimer HOMO and HOMO−1 (LUMO and LUMO+1) and the interactions of monomer HOMOs (LUMOs). The Kohn−Sham Hamiltonian was obtained from the secular equation, $\mathcal{H} = \mathbf{SCEC}^{-1}$ by the fragment molecular orbital (FMO) approach with B3LYP density functional method along with 6-311G(d,p) basis set, where the diagonal elements are the site energies $e_{1(2)}$ and off-diagonal elements are the charge-transfer quantity, J_{12}, both in a nonorthonormal basis. When we transform the J_{12} to an orthonormal basis, we get the effective charge hopping element, J_{12}^{eff} in the following equation, which is similar to the J_{12} given above.

$$J_{12}^{\mathrm{eff}} = \frac{J_{12} - \frac{1}{2}(e_1 - e_2)S_{12}}{1 - {S_{12}}^2}$$

when the HOMOs are used $J_{12}^{\mathrm{eff}} = J_{\mathrm{H}}$ and the when LUMOs are used $J_{12}^{\mathrm{eff}} = J_{\mathrm{L}}$.

We have also computed the transfer integral for hole and electron transport using the energy splitting in dimer (ESID) method. Here the transfer integral is estimated as half of the difference between the energy values of HOMO and HOMO−1 for hole transport and half of the difference between the energy values of LUMO and LUMO+1 for electron transport.[53−57] It is known that ESID is not a rigorous method, but nevertheless in some cases we find very good agreement with the results obtained using the EDH method.[24,23]

To explain the anisotropy of conduction, we have investigated the relative binding energies of all the intermolecular dimer orientations extracted from the crystal structure. The interlayer interaction energies are noncovalent in nature, and the DFT description of these interactions requires long-range dispersion-corrected functionals. The interaction (association) energy ΔE is obtained from single-point calculation using three different functionals, namely the M06-2X, dispersion-corrected B97-D functional, and the double hybrid functional, B2PLYP-D DFT, methods.[58−61] We use a Pople's split valence 6-311G(d,p) for C, N, H, and F and 6-311G(3df,3pd) for S basis set. The ΔE is calculated using the following equation

$$\Delta E = E_{\mathrm{AB}} - E_{\mathrm{A}} - E_{\mathrm{B}}$$

where E_{AB} is the total energy of a pair of molecules in the crystal and E_{A} and E_{B} are the single-point energies of the isolated monomer A and B extracted from the crystal coordinates. Counterpoise (CP) correction for basis set superposition error (BSSE) has been included only for the B2PLYP-D method, as it contains a perturbative contribution to the correlation energy, while for the other methods the BSSE is expected to be small.[62,63] Accurate interaction energies have been known to be obtained when half of counterpoise correction is added to ΔE.[64] Hence we apply this formula here for the B2PLYP-D calculations.

The electronic band structure and charge densities of the organic crystals have been calculated using Quantum Espresso Program Package.[65] The calculations have been performed within the framework of the density functional theory (DFT) with the use of the calculated fundamental basis set consisting of plane waves and pseudopotentials. We make use of generalized gradient approximation (GGA) DFT PBE (Perdew−Burke−Ernzerh) exchange and correlation functional.[66] The effect produced by the core electrons was taken into account through the use of Ultrasoft Vanderbilt pseudopotentials and with an energy cutoff of 65 Ry for the wave function (520 for the electron density) for 2, with a K point mesh of 10 × 4 × 3. In order to obtain the band structure, we carried out additional non-self-consistent field (non-SCF) across some selected high-symmetric k paths.

RESULTS AND DISCUSSION

Geometric Structure. The crystal structure data were retrieved from the Cambridge Structural Database (CSD) for five molecules, namely, **1**, **2**, **3**, **4**, and **7**.[34−38] The DFT estimates of geometric parameters of these five molecules are compared with the experimentally determined ones obtained from the literature in Table 1. The other geometrical parameters of the central ring and the exocyclic bonds are given in the Supporting Information. For **2** there are two orthogonal half-units (A and B) in the asymmetric unit which differ in geometry. Hence two sets of bond parameters as determined from experiment are shown. The molecules **2**−**4** exhibit rigid skeletons. Molecules with substitution at the 2,6-positions, where the groups are directly attached to the central ring BBTz, are almost planar and hence create a good conjugation. Only in the case of extended conjugation in **4** the planarity is lost—there is a small angle

dx.doi.org/10.1021/jp304892x | J. Phys. Chem. C 2012, 116, 22663−22674

between the thiophene and the trifluoromethyl phenyl group. This angle is overestimated by theory: while the experimental determined value is 5°, the theoretical value is 25°.[37] On the other hand, the 4,8-substituted **7** develops an angle (21° experiment and 33° theory) even between the substituted group and the central BBTz ring.[38]

Generally, it is well-known that results of DFT methods compare well with the bond lengths obtained from experiment. For the molecules here, most of the theoretical estimated bond parameters are in good agreement with the experimentally determined ones. For example, in **1** for all the bond parameters, the deviations between the theoretical generated values and the experimental measured values are within 0.010 Å. On the other hand in **2,** which has two inequivalent molecules in the unit cell, the deviations are much smaller when comparison is carried out with one of the molecules (B) but when the comparison of the bond parameters is carried out with the other molecule (A) in the asymmetric unit the deviations are larger notably in the r_4(C−S) bond and r_7(C−C) bond lengths. In **3** the r_1(C−N) bond length deviates by 0.034 Å while in **4** it is the r_3(C−S) bond length that deviates by 0.027 Å. There are no major deviations in **7**. Overall, the deviations could be attributed to the intermolecular interactions in the crystal.

The main interest in the geometry would be to look into the changes of the central ring, BBTz, or in other words **1** upon substitution. The changes in geometrical parameters are presented in Figure 1 only for the gas-phase data (computed).

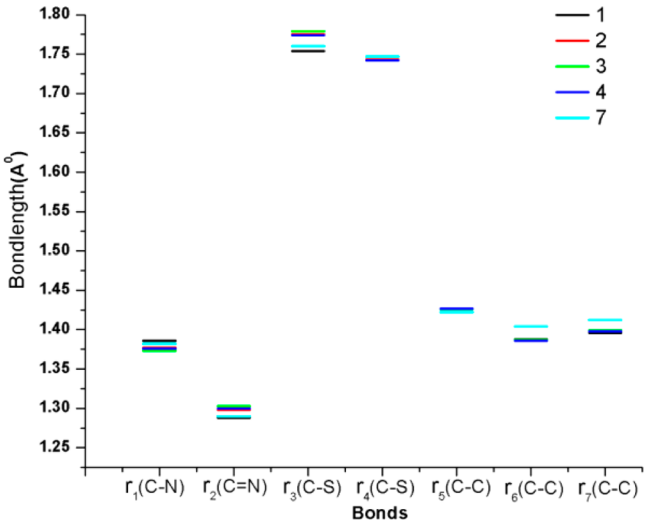

Figure 1. Changes in geometrical parameters, upon substitution, of **1** obtained at B3LYP/6-311G(d,p) for C, N, H, and F and 6-311G(3df,3pd) for S. See Scheme 1 for bond numbering.

From the figure it is clear that the r_1(C−N) bond is shortened while the vicinal bonds (r_2(C−N) and r_3(C−S)) are slightly elongated upon substitution. The r_5(C−C) and the r_4(C−S) bonds hardly change on substitution. This is also true for r_6(C−C) and r_7(C−C) with the exception of **7** which shows larger change.

HOMO, LUMO, IP, and EA. Charge carrier (hole/electron) injection properties can be ascertained on a relative basis from the knowledge of energies of the frontier orbitals (HOMOs and LUMOs) and the IP/EA values.[43] Keeping this in view, we investigate the changes that take place to the frontier orbitals upon substitution. The calculated HOMO, LUMO eigenvalues and the HOMO−LUMO gaps (HLG) are shown in Table 2. The HOMO and LUMO orbital plots are given in Figure 2, and it is evident that both are of π nature spread over the entire molecular skeleton. The molecules **1**−**4** have almost similar HOMO and LUMO, but in the case of **7** this changes due to the substitution. The HOMO and LUMO energies of the unsubstituted molecule, **1**, lie at −6.5 and −1.89 eV, respectively, and a reasonably large HLG of 4.6 eV is obtained. Introduction of a group like thiophene at the 2,6-position destabilizes the HOMO energy level of **1** to −5.79 eV as seen in **2**. On the other hand, the LUMO is stabilized to −2.31 eV. As expected, the increase in the conjugation leads to a smaller HLG of 3.48 eV. **3** has an almost similar HOMO and LUMO and its HLG is 3.21 eV. Experimental data determined by electrochemical methods are available for **2** and **3**.[35,36] The experimentally extrapolated HOMO and LUMO values for **2** are −6.0 and −2.7 eV and for **3** are −5.7 and −2.9 eV, respectively, which are in reasonable agreement with the calculated values. On the other hand, for **4** we see a slightly destabilized HOMO, while the LUMO is largely stabilized (as expected due to the electron-withdrawing nature of the substituent). The HLG is slightly smaller and it is 3.13 eV. Overall, it is seen that the 2,6-substituted derivatives induce large changes in the HOMO and LUMO eigenvalues. Hence the end substituents provide a wide flexibility in tuning the electronic properties of the BBTz derivatives. In the case of **7** we see that the LUMO value is slightly lower (by 0.09 eV) when compared to the bare molecule. Slightly larger change is seen in the case of HOMO which is 5.53 eV when compared to the bare molecule's 6.5 eV. The HLG in this case is 3.55 eV. Of this series, **7** has the largest HLG.

Vertical and adiabatic IP and EA calculated using ΔSCF method are given in the same table. The bare molecule has a large IP of 8.14 eV which decreases to 6.96 eV when substituted with groups like thiophene at the 2- and 6-positions (**2**). It further drops to 6.57 eV in the case of **3**. For **4** the value is almost same as that of **2** though it has a electron-withdrawing group. **7** has a smaller IP when compared to **2**. The adiabatic IP follow similar trend. Vertical EA also is seen to be smallest in **1** which becomes larger with substitution. For **2** the EA is 1.04 eV which increases to 1.22 eV in **3**. The largest value in this series is for **4**, the n-type semiconductor, indicating that it would be ideal for electron injection. On the other hand, **7** has a very small EA and is almost similar to **1**. As in the case of IP, here too the adiabatic EA follow the vertical EA trend. To check the effect of adding diffuse functions to the calculations in the case of anions, we recalculated the AEA/VEA using the basis set 6-311+G(d,p) for all atoms except for sulfur where 6-311+G(3pd,3df) was used. The results are shown in the Supporting Information. The values are slightly larger than the ones given in Table 2, but the trends remain same.

Geometry Changes upon Oxidation and Reduction. The geometry changes which the molecules undergo during an oxidation and reduction process are projected graphically in the Supporting Information. It is clearly seen that upon oxidation the bare molecule undergoes minor modifications in bond length of bonds r_4(C−S), r_5(C−C), and r_6(C−C) while r_2(C−N) and r_7(C−C) elongate by about 0.025 Å. The bonds r_1(C−N) and r_3(C−S) shorten by 0.03 Å. The 2,6-substituted derivatives (**2**−**4**) behave differently from **1** but have similarities with each other. We notice that the changes in bond length are very small in the C−S bonds. The r_2(C−N), r_5(C−C), and r_7(C−C) bonds elongate while r_1(C−N), r_6(C−C), and r_8(C−C) shorten upon oxidation. **7** behaves in slightly different manner from **2**−**4**. We see a shortening of the bond length r_5(C−C) upon oxidation

dx.doi.org/10.1021/jp304892x | J. Phys. Chem. C 2012, 116, 22663−22674

Table 2. Calculated and Experimentally (Where Available) Determined HOMO, LUMO, and HLG Values along with Vertical Ionization Potential (VIP), Vertical Electron Affinity (VEA), Adiabatic Ionization Potential (AIP), and Adiabatic Electron Affinity (AEA), for 1−4 and 7

	calculated (in eV)[a]			experiment (in eV)[c]						
molecule	HOMO	LUMO	HLG	HOMO	LUMO	HLG	VIP (eV)[b]	VEA (eV)[b,d]	AIP (eV)[b]	AEA (eV)[b,d]
1	−6.5	−1.89	4.6	–	–	–	8.14	−0.11	8.07	−0.26
2	−5.79	−2.31	3.48	−6	−2.7	3.3	6.96	−1.04	6.81	−1.15
3	−5.54	−2.33	3.21	−5.7	−2.9	2.8	6.57	−1.22	6.43	−1.32
4	−5.98	−2.85	3.13	–	–	–	6.95	−1.75	6.81	−1.91
7	−5.53	−1.98	3.55	–	–	–	6.76	−0.65	6.58	−0.87

[a]Data obtained from single-point calculations at B3LYP/6-311++G(d,p) for C, N, H, and F and 6-311++G(3df,3pd) for S using the optimized geometries. [b]The basis set used is 6-311G(d,p) for all the atoms; sulfur atom is further augmented with 3df,3pd polarization. [c]References 35 and 36. [d]Values obtained by adding diffuse functions to the calculation in the case of anions are given in Supporting Information.

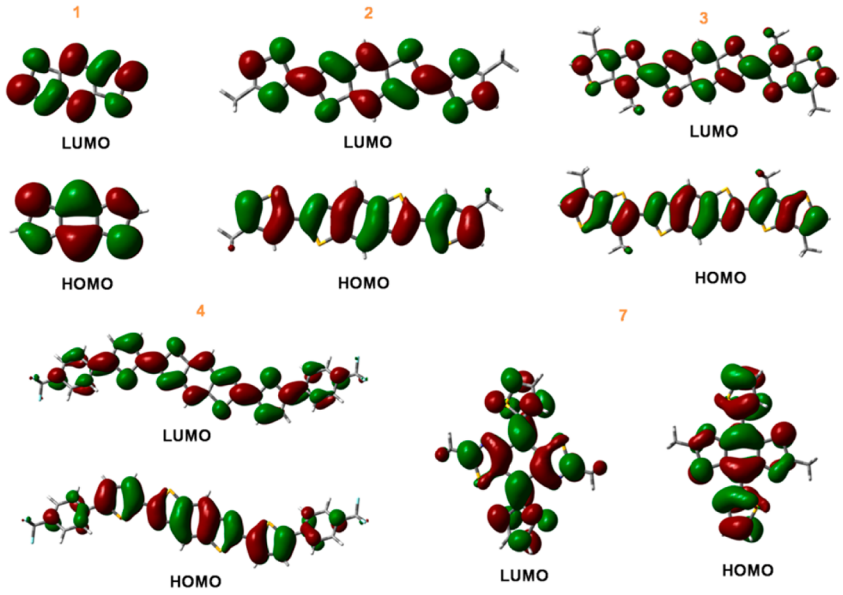

Figure 2. Frontier MOs of **1**−**4** and **7** molecules obtained at B3LYP/6-311G (d,p) for C, N, H, and F and 6-311G(3df,3pd) for S.

Table 3. Theoretical Estimation of the Reorganization Energies (meV) λ_+ (Hole Transport), λ_- (Electron Transport) of 1− 4 and 7 along with λ_1, λ_2, λ_3, and λ_4 Obtained at the B3LYP/6-311G(d,p) for C, N, H, and F and 6-311G(3pd,3df) for S[a]

molecule	λ_1	λ_2	λ_+	λ_3	λ_4	λ_-[b]
1	63 (74)	98 (99)	162 (173)	151 (150)	156 (158)	307 (308)
2	159 (159)	162 (167)	321 (326)	106 (106)	105 (109)	211 (215)
3	136 (137)	147 (146)	283 (283)	91 (90)	93 (92)	184 (182)
4	136 (135)	141 (143)	277 (278)	163 (160)	136 (184)	299 (344)
7	183 (186)	151 (154)	334 (340)	224	113	337

[a]Values given in parentheses are obtained from normal-mode analysis. [b]Values obtained by adding diffuse functions to the calculation in the case of anions are given in the Supporting Information.

while r_6(C−C) elongates. The shortening of r_1(C−N) is also much smaller when compared to the other derivatives.

In the case of reduction we see that r_7(C−C) and r_1(C−N) bond changes are the maximum in the bare molecule. While the former elongates, the latter shortens. The bond r_2(C−N) also undergoes a large elongation upon reduction. In the case of 2,6-substituted derivatives the bonds r_3(C−S) and r_4(C−S) elongate unlike in the case of oxidation. The largest changes are seen in r_1(C−N) and in r_8(C−C) as in the case of oxidation. Here r_6(C−C) bond hardly changes upon reduction except in **7** where it elongates. From the geometric changes upon oxidation and reduction one can expect large reorganization energies for these molecules.

Reorganization Energies (Electron−Vibration Coupling). Local coupling and nonlocal coupling are the two main electron−vibration/electron−phonon interactions that occur in organic crystals.[23] These two couplings are usually estimated to understand the charge transport in the semiconductor.[52] While nonlocal coupling is usually estimated by transfer integrals between the neighboring molecules in the crystal, local coupling is usually estimated by calculation of the intramolecular reorganization energy. Estimated reorganization energies as obtained from DFT calculations are shown in Table 3. Both the hole− and electron−vibrational couplings obtained using Scheme 2 (adiabatic potentials) and the values obtained from normal-mode analysis are shown in the same table. One can

dx.doi.org/10.1021/jp304892x | J. Phys. Chem. C 2012, 116, 22663−22674

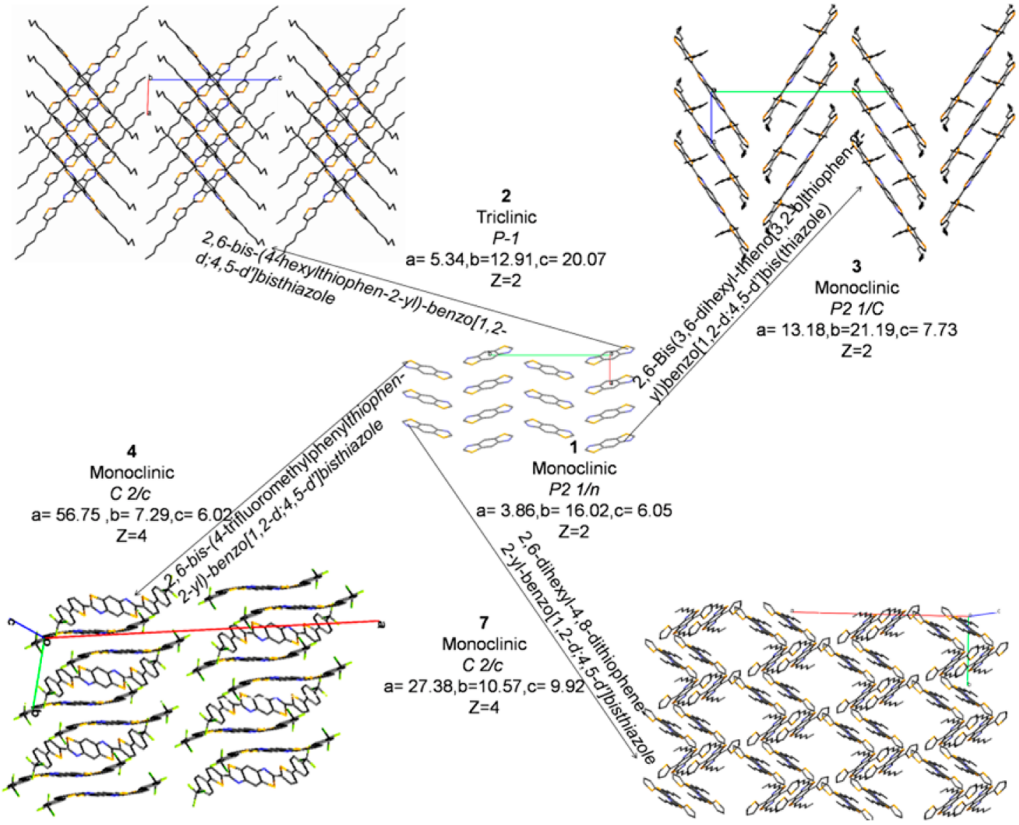

Figure 3. Crystal packing diagrams for **1**−**4** and **7**.[34−38]

observe that the results of these two methods are nearly in good agreement with each other.

The calculated electron reorganization energy for the bare molecule **1** is 307 meV while for the hole the reorganization energy is only 162 meV. We compare this with pentacene which is known to be a very good semiconductor. Pentacene's hole reorganization energy is 97 meV while its electron reorganization energy is 136 meV (at B3LYP/6-311G(d,p) level of theory).[67] Thus, even the bare molecule **1** has around 2 times larger reorganization energies. Relatively, **1** should transport holes better than electrons. The vibrational couplings related to the hole and electron mobilities of this molecule are shown in the Supporting Information. It is clear from this figure that the transfer is dominated by the high-energy modes. For example, in the case of hole transport the vibrational mode at 1500 cm^{-1} is the most dominant one, while for the electron transport the vibrational modes at 1580 and 1370 cm^{-1} are the most dominant ones. The larger reorganization energy for electron transport is due to the larger contribution from these peaks.

In the case of substituted p-type molecules **2** and **3**, we observe that the reorganization energies for the electron transport is much smaller, for example in **2** we observe that the reorganization energy is 211 meV while for **3** it is 184 meV. For the hole transport it is 321 and 283 meV, respectively. We note from the Supporting Information that the high-energy vibrational modes are dominant in **2** but in addition in the case of hole transport a low vibrational mode also dominates. This is also seen in **3**. In **4** the reorganization energy for hole transport is slightly lower in energy compared to the reorganization energy for electron transport, i.e., 277 meV compared to 299 meV. It is interesting to note that the hole transport reorganization energy is lower in **4** which is an n-type semiconductor. From the normal-mode analysis we find that these are dominated by the high-energy vibrations. In **7** both hole transport and electron transport require high energy and are in the range 334 and 337 meV. The vibrational contribution to this reorganization energy is available only for hole transport and it is clear that the along with the high-energy modes some lower energy vibrations also contribute.

From the reorganization energy calculations it is found that the local coupling in these fused heterocyclic ring systems is large and these are almost 2−3 times larger than good semiconducting materials like pentacene and ruberene. In other words, at the molecular level, based on the reorganization energies, these molecules cannot be classified as n- or p-type semiconductors. It is also seen that the reorganization energy which is one of the key parameters in electron transfer does not correlate here with the experimental observed semiconduction, pointing to the fact that nonlocal coupling and IP/EA are probably playing the major roles. To check the effect of adding diffuse functions to the calculations involving anions (for electron transport), we recalculated λ_- using the basis set 6-311+G(d,p) for all atoms except for sulfur where 6-311+G(3pd,3df) was used. The results are shown in the Supporting Information. The values are almost similar to the ones given in Table 3.

Crystal Analysis. We carried out further detailed studies of molecules **1**−**4** and **7** at the solid-state level. The crystal packing along with the structural details are shown in Figure 3. Crystal **1** belongs to the monoclinic crystal system with lattice parameters a = 3.861 Å, b = 16.025 Å, and c = 6.053 Å. Its space group is $P2_1/n$.[34] The unit cell contains two molecules. The molecules arrange in a herringbone pattern. The distance between the two molecules which are slipped cofacial in the a direction is about 3.86 Å. In the direction b the nearest atom contacts are between the S and the N which is about 3.425 Å. In the c direction the

dx.doi.org/10.1021/jp304892x | J. Phys. Chem. C 2012, 116, 22663−22674

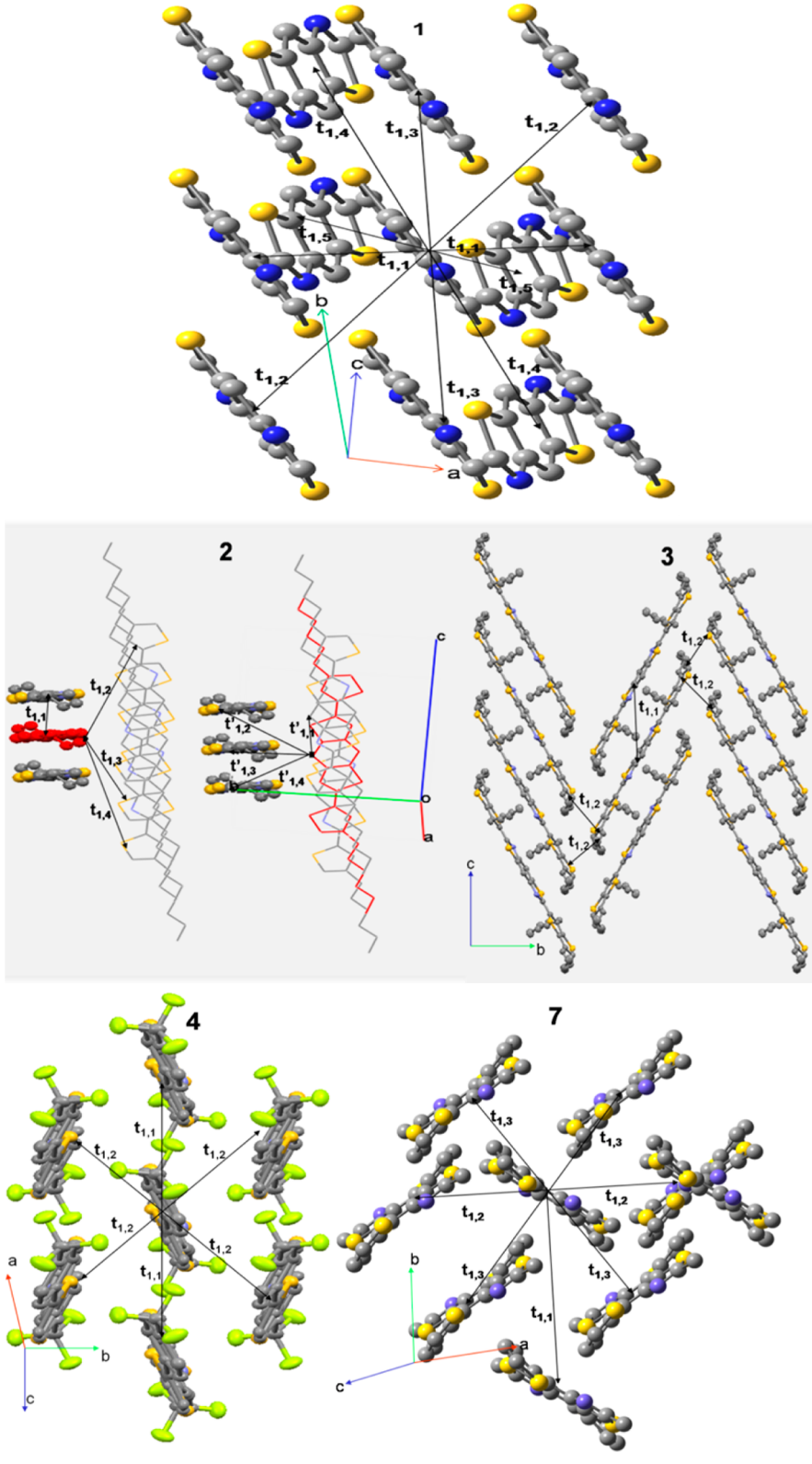

Figure 4. Dimers for which the charge transfer parameter and interaction energy have been calculated.

nearest atoms contacts are the S−N contact which is 3.81 Å and S−S contact which is about 6.436 Å.

Crystal **2** belongs to a triclinic crystal system and its space group is $P\bar{1}$.[35] The asymmetric unit contains two orthogonal half-units which are not equivalent. Each orthogonal molecule assembles into a cofacial slipped stack arrangements making an inter-ring $\pi-\pi$ contact. The distance between two cofacial molecules in the direction *a* is 5.343 Å. In the direction between *a* and *b* we have another molecule which is orthogonal to the first molecule. This molecule also has a distance of 5.343 Å with its cofacial neighbor. In the direction *b* we have S−N contact of 3.016 Å and S−S nearest-neighbor contacts with a distance of

dx.doi.org/10.1021/jp304892x | *J. Phys. Chem. C* 2012, 116, 22663−22674

3.735 Å. The S−N distance is shorter than the combined van der Waals radii for the two interacting atoms.[35]

In the case crystal of **3** we can see molecules aggregate themselves into columns of slipped cofacial arrangement with a herringbone π stacking assembly as shown in Figure 3. This type of packing should give a larger noncovalent interaction with its neighbors due to the tilt which nevertheless retains the $\pi-\pi$ overlap. This molecule also belongs to monoclinic crystal system and its space group is $P2_1/c$.[36] It has two molecules in the unit cell. The distance between the slipped cofacial packed molecules in the c direction is around 7.712 Å. The distance between the molecules which are tilted (centroid to centroid) is 11.269 Å in the direction b. In the direction a the atom−atom contacts are farther away.

In **4** the molecule lies along the a axis, which has a lattice parameter of 56.75 Å.[37] This crystal belongs to the monoclinc crystal class and the space group is $C2/c$. It has four molecules in the unit cell. In the direction b the molecules interact in a tilted manner with the distance of about 4.727 Å between them (a herringbone pattern). In the direction c the distance between the molecules which are more cofacial is 6.020 Å. The nearest atom−atom contacts are in the a direction between the CF_3 and CF_3, which is 2.854 Å.

In **7**, due to the large hexyl chain in each molecule, the molecules do not pack in a cofacial manner and hence the nearest neighbors which are parallel stacked are translated along the short molecular axis leading to reduced $\pi-\pi$ interaction.[38] The other neighboring molecule interacts in a T-shaped manner. The molecules crystallize into monoclinic crystal system having a space group $C2/c$. It has four molecules in the unit cell. In the direction c the distance between the slipped cofacial molecules is around 9.916 Å. In the a direction the nearest-neighbor contacts are much larger. In the b direction the centroids are about 6.772 Å distant.

Transfer Integral in Crystal. We now turn our focus to the transfer integral (nonlocal coupling), the other important parameter governing the charge transport performance. The transfer integrals are estimated for the plausible near-neighboring pairs of molecules in the crystals as shown in Figure 4 using B3LYP functional with a moderate split valence and polarization basis set, 6-311G(d,p) using both EDH and ESID methods. Only the dominant values obtained using the EDH method are shown in Table 4 while those calculated by the ESID method are given in the Supporting Information. The interaction integral in the $t_{1,1}$ direction for the bare molecule, **1**, is 62 meV for hole transport while in the same direction the electron transport drops to 28 meV. These molecules are separated by a distance of 3.86 Å. On the other hand, in the pathway $t_{1,2}$, $t_{1,3}$, $t_{1,4}$, and $t_{1,5}$ the transfer integrals are much smaller. To understand the reason for the larger values for the $t_{1,1}$ pathway, we look into the frontier orbitals of the dimer given in the Supporting Information. It is clear that there is a near cofacial type of stacking in the $t_{1,1}$ pathway. This leads to a larger splitting of the energy between the HOMO and the HOMO−1 due to stronger bonding interactions in the HOMO−1 and antibonding interactions in the HOMO of the dimer. From the frontier orbital pictures it is also clearly seen that the stronger interaction between the HOMOs of the individual molecules when compared to the interaction between the LUMOs leads to larger transfer integral for the hole transport. In the other pathways for example in $t_{1,2}$ the molecules hardly have any $\pi-\pi$ interaction due to the large distance. In the case of $t_{1,3}$ the individual molecules in the dimer are translated along the short axis leading to slightly weaker interaction between the orbitals. Thus, the interaction integral obtained for hole transport is around 10 meV while for electron transport is 11 meV. In $t_{1,4}$,in the direction of b axis, though the distance is 8.81 Å between the centroids, the molecules are almost lying side by side with the S−N distance being 3.42 Å. This arrangement leads to slightly larger splitting in the LUMOs and thus we obtain 15 meV for electron transport and 10 meV for hole transport. In the pathway $t_{1,5}$ the molecules hardly have any $\pi-\pi$ interaction, leading to very small transfer integrals.

Table 4. Estimation of Hole (J_H) and Electron (J_L) Transfer Integrals for the Molecules 1− 4 and 7 (in meV) at B3LYP/6-311G (d,p) Level of Theory Using EDH Method[a] along with the Rate Constants (in s^{-1})

molecule	dimer	d^b	J_H	k^+ (s^{-1})	J_L	k^- (s^{-1})
1	$t_{1,1}$	3.86	62	3.35×10^{13}	28	1.24×10^{12}
	$t_{1,2}$	7.05	2	2.82×10^{10}	1	9.96×10^{8}
	$t_{1,3}$	6.05	11	9.79×10^{11}	11	1.93×10^{11}
	$t_{1,4}$	8.81	10	8.41×10^{11}	16	3.81×10^{11}
	$t_{1,5}$	8.75	3	7.67×10^{10}	2	6.47×10^{9}
2	$t_{1,1}$	5.34	193	4.95×10^{13}	34	5.61×10^{12}
	$t'_{1,1}$	5.34	104	1.45×10^{13}	23	2.54×10^{12}
	$t_{1,2}$	9.18	2	5.16×10^{9}	22	2.39×10^{12}
	$t_{1,3}$	6.46	1	1.36×10^{9}	16	1.25×10^{12}
	$t_{1,4}$	7.50	3	1.56×10^{10}	9	4.07×10^{11}
3	$t_{1,1}$	7.73	67	9.27×10^{12}	32	6.93×10^{12}
	$t_{1,2}$	11.28	2	1.04×10^{10}	7	3.23×10^{11}
4	$t_{1,1}$	6.02	8	1.42×10^{11}	31	1.60×10^{12}
	$t_{1,2}$	4.73	22	1.05×10^{12}	11	2.05×10^{11}
7	$t_{1,1}$	9.92	–	2.58×10^{05}	3	8.40×10^{09}
	$t_{1,2}$	13.17	16	3.05×10^{11}	11	1.34×10^{11}
	$t_{1,3}$	7.25	5	3.39×10^{10}	8	7.18×10^{10}

[a]Values obtained from the ESID are given in the Supporting Information. [b]d (Å) represents intermolecular center-to-center distance.

2 is obtained from **1** by attaching a thiophene ring to the bare moiety. The intramolecular S−N contacts which are about 2.98 Å tend to retain the planarity of this molecule, thus yielding a larger π-conjugated system. The extra thiophene ring helps in additional intermolecular S−N close contacts which leads to $\pi-\pi$ stacking in the crystal. This should be helpful for increasing the charge transfer. Since in the crystal the asymmetric unit consists of two half molecules which are not equivalent, we obtain two complete molecules which differ due to the conformation of the hexyl chain, the transfer integrals for which are distinguished as t and t'. The $t'_{1,1}$ is very large for the hole transport, i.e., 193 meV, but it drops down drastically to 34 meV for electron transport. For the other molecule the transfer integral, $t_{1,1}$ is slightly smaller though the distance is the same, 5.34 Å. Here it is 104 meV for hole transport and 23 meV for electron transport. To understand the difference in the absolute magnitude of the transfer integral in the dimers of these two molecules (though the centroid to centroid distances remain the same), we analyze the distances in the dimers. We note that in the first molecule ($t'_{1,1}$ case) the intermolecular S−N distance is 3.7 and 3.79 Å which is closer when compared to the S−N distance of 4.06 and 3.96 Å in the case of the second molecule ($t_{1,1}$). The S−S distances are 5.37 Å in the first molecule and 5.81 Å in the second molecule. The diagonally opposite N−N distances are also different (4.21 Å in the first molecule compared to 4.93 Å in the second molecule). Thus, it is clear that the transfer integral is enhanced in the first molecule due to closer heteroatom contacts.

dx.doi.org/10.1021/jp304892x | J. Phys. Chem. C 2012, 116, 22663−22674

Values of 9−22 meV for electron transport are obtained for the other directions $t_{1,2}$, $t_{1,3}$, and $t_{1,4}$, but they are very small compared to the values obtained for the $t_{1,1}$ and $t'_{1,1}$ directions.

3 is obtained from **1** by addition of a fused dialkylthienothiophene end units. Though the intramolecular S−N contacts help in retaining the planar conformation due to the presence of the dialkyl units, the molecules in the crystal pack in a herringbone formation, thus reducing the larger cofacial arrangement as seen in **2**. The transfer integral for hole transport is also larger in this crystal than the electron transport. A value of 67 meV is obtained for hole transport, while for electron transport it is 32 meV. In the direction $t_{1,2}$ the transfer integrals are very small as expected due to the v-shape interaction. In the case of **4**, due to the extra phenyl ring attached to the thiophene there is small loss of planarity of the molecule. Due to this the cofacial arrangement is absent. As per experimental reports this is an electron-transporting material and we find that the transfer integral is larger for electron transport, i.e., 31 meV, while the hole transport transfer integral is very small, 8 meV in the $t_{1,1}$ direction. The $t_{1,2}$ shows a larger value of 21 meV for hole transfer compared to electron transfer of 11 meV. From the frontier orbitals of this molecule given in the Supporting Information, it is clearly seen that in the case of $t_{1,1}$ direction the dimer is not cofacial but translated to one side on its short axis, leading to larger bonding in the case of individual LUMO interactions. In the case of the direction $t_{1,2}$, the dimer is in a tilted conformation which leads to again to a slightly larger interaction between the individual monomer HOMOs. In **7**, for both electron and hole transfer, the transfer integrals are small. The largest are ∼16 meV for hole transport and 11 meV for electron transport in the $t_{1,2}$ direction. The smaller values here are due to larger distances between the individual monomers and the lack of a cofacial type of packing.

From these calculations it is clear that the transfer integral is the main parameter in these molecules to understand the nature of semiconduction. For example, **2** which has been classified as a p-type semiconductor shows a very large transfer integral value of 193 meV for hole transport in one direction and in the other direction it is 104 meV. The corresponding transfer integral for electron transport drops down to 34 and 23 meV, indicating the dominance of hole transport in the crystal. On the other hand, **4** which has been classified as n-type semiconductor shows a larger value of the transfer integral for electron transport when compared to the transfer integral for hole transport. Similarly, on the basis of the results we can classify the yet to be investigated **7** as p-type semiconductor. Finally, as expected, we note that the values of transfer integral are in good agreement with those obtained by ESID method only for some pathways. In these cases the good agreement can be attributed to the HOMO(LUMO) and HOMO−1(LUMO+1) orbitals of the dimer containing contribution exclusively from the monomer HOMOs-(LUMOs).[23]

Rate constants calculated using the Marcus formula at $T = 300$ K are also shown in the same table. The largest value obtained is for the hole transport along the $t_{1,1}$ pathway of **2** . This is 4.95×10^{13} s^{-1}. The rate constants for the electron transport are slightly smaller. In agreement with the above discussion, the rate constants follow the transfer integral trend.

Interaction Energies. Keeping in view the interesting results shown above, we decided to investigate the noncovalent interactions between the molecules of the dimers in the solid state. The values (ΔE) are calculated using three different methodologies, namely B2PLYP-D(BSSE corrected), B97-D, and M06-2X, and these are summarized in Table 5. The uncorrected interaction energies obtained by the B2PLYP-D method along with the CP corrections are shown in the Supporting Information. The trends obtained with these three DFT methods are similar. In the case of **1** the largest ΔE of about 9.78 kcal/mol is obtained for face-to-face arrangement (distance between monomers separated by about 3.86 Å) using the B2PLYP-D functional. For the same dimer, the ΔE predicted by using B97-D is 10.5 kcal/mol while with M06-2X a ΔE of 11 kcal/mol is obtained. The $t_{1,3}$ interaction in this molecule is of a much smaller order and a value of 3.8 kcal/mol is obtained using B2PLYP-D. The M06-2X value here is 3.2 kcal/mol. The interaction in the direction of $t_{1,5}$ with a distance of ∼8 Å is the lowest and it is around 1.8 kcal/mol. Interaction energies calculated for **2** using B2PLYP-D in the direction $t_{1,1}$ is 20.0 kcal/mol, while the predicted value using B97-D is 21.6 kcal/mol. The M06-2X predicts a ΔE which is almost similar to the one predicted by B97-D. In the second molecule which is inequivalent to the first one, we obtain a ΔE of 18.06 kcal/mol for the parallel stacking using the B2PLYP-D functional. Here the M06-2X predicted value is also around 18.5 kcal/mol. In the interaction direction $t_{1,2}$ and $t_{1,3}$, which would be the side-by-side interaction, the B2PLYP-D predicts a value of 5.9 kcal/mol while here the M06-2X values are slightly smaller. Thus, the presence of the extra thiophene ring in **2** compared to **1**, due to the retention of planarity, has almost double the interaction energy for the near-parallel stacked conformation. The $\pi-\pi$ interaction energy predicted for **3** is the largest in the series and its value is 23.7 kcal/mol when B2PLYP-D functional is used. Here the M06-2X yields a value of 24.4 kcal/mol. The additional ring due to the fused ring system, thienothiophene, retains the planarity and thus a larger area for interaction is available in the dimer. The larger interaction energies in **3** rather than in **2** which is actually cofacial can also be attributed to the larger repulsion in the latter while there is a stabilization in the former due to the tilt.[36] The interaction energies of **4** are the smallest in the substituted series in the direction $t_{1,1}$. The predicted value using B2PLYP-D is 15.7 kcal/mol. There is a drastic drop in the M06-2X value and it yields only 11.6 kcal/mol. The B97-D value of 18.4 kcal/mol.

Table 5. Interaction Energies (ΔE, kcal/mol) for 1−4 and 7 Using B2PLYP-D, B97-D, and M06-2X Using 6-311G(d,p) for C, N, H, and F and 6-311G(3df,3pd) for S

		ΔE		
molecule	dimer	B2PLYP-D[a]	B97-D	M06-2X
1	$t_{1,1}$	9.8	10.5	11.0
	$t_{1,2}$	0.5	0.7	0.03
	$t_{1,3}$	3.8	4.2	3.2
	$t_{1,4}$	4.4	4.4	4.1
	$t_{1,5}$	1.8	2.2	1.3
2	$t_{1,1}$	20.0	21.6	21.8
	$t'_{1,1}$	18.1	20.3	18.5
	$t_{1,2}$	5.9	6.0	4.5
	$t_{1,3}$	4.7	4.3	4.3
	$t_{1,4}$	2.9	3.2	1.43
3	$t_{1,1}$	23.7	25.0	24.4
	$t_{1,2}$	5.3	5.9	4.6
4	$t_{1,1}$	15.7	18.4	11.6
	$t_{1,2}$	23.8	28.4	21.9
7	$t_{1,1}$	3.6	4.4	3.0
	$t_{1,2}$	1.9	2.5	1.5
	$t_{1,3}$	8.5	9.6	7.8

[a]BSSE corrected (ΔE + 1/2 CP).

Here the $t_{1,2}$ has a large value of 23.8 kcal/mol as predicted by B97-D. The interaction energy, 21.9 kcal/mol, predicted by M06-2X is almost 2 kcal/mol different as in the $t_{1,1}$ case. Here, in **7** the interaction energies obtained are very small comparatively, the largest being 8.5 kcal/mol in the $t_{1,3}$ direction. M06-2X predicts slightly lower value of 7.7 kcal/mol. Here the alkyl chains attached to the thiophene ring seem to play a major role; they do not allow close interaction of the dimers. Thus, near-parallel stacking as observed for other molecules is absent in this case. Overall, it is seen that the values predicted by M06-2X are smaller.

Band Structure. The electronic band structure of **2** is shown in Figure 5. The band structures are plotted along specific directions of the first Brillouin zone. The band gap obtained by the plane wave method is 1.75 eV which is at the Γ point. This is smaller compared to the experimental value of 3.3 eV.[35] To understand whether this underestimation is due to the well-known DFT problem, we recalculated at the Γ point the band gap using the hybrid functional PBE0.[68] This was carried out using Crystal09 software.[69,70] The band gap obtained is 2.72 eV which matches well with the experimental results. It should be pointed out that though the PBE functional underestimates the band gap, the main characteristics of valence and conduction band will not be affected.[25]

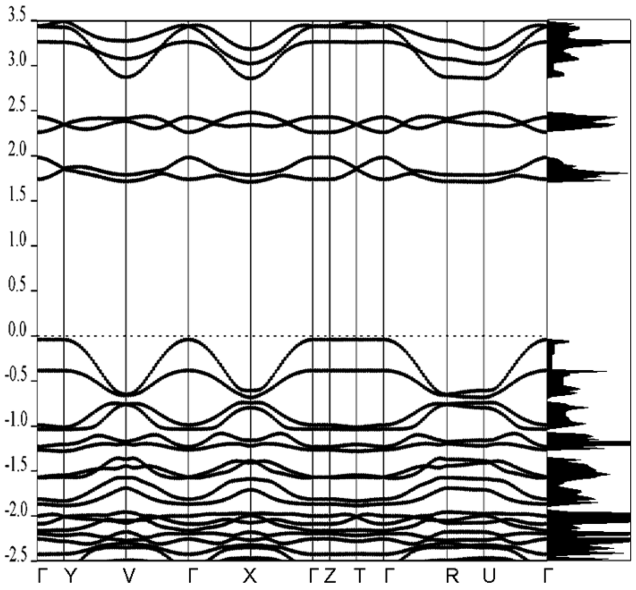

Figure 5. Plotted electronic band structure of **2** along the high symmetric *k*-points in the first Brillouin zone which are labeled accordingly as Γ = (0,0,0), *Y* = (0,1/2,0), *V* = (1/2,1/2,0), *X* = (1/2,0,0), *Z* = (0,0,1/2), *T* = (0,1/2,1/2), *R* = (1/2,1/2,1/2), and *U* = (1/2,0,1/2). Fermi energy to the top of valence band is aligned to zero. Its corresponding density of states is also plotted to the right of the band structure.

The valence band consists of two nearly degenerate π sub-bands. The presence of which is attributed to the two inequivalent molecules in the unit cell. Similarly, the conduction band also has the near-degenerate π sub-bands. The bandwidth of the valence band is 620 meV and that of conduction band is only 260 meV. The larger dispersion of the valence band is along the axis which corresponds to Γ*X* in the figure. The band is almost flat in the Γ*Y* and Γ*Z*. These values correspond to the sulfur−sulfur interaction. Only in the diagonal directions, namely, the Γ*U* and Γ*V*, the dispersion is again large. The values obtained are consistent with the transfer integral data.

CONCLUSIONS

In this study, we evaluate at both the molecular level and solid-state level the recently suggested BBTz derivatives, for OFET applications, using computational techniques. Our calculations indicate that the molecules have largely similar geometry in the gas phase and solid state with the basic core remaining mostly planar. We observe that these fused BBTz derivatives at the molecular level are not in the same class of semiconductors as pentacene or rubrene, for they show large reorganization energies which are almost 2−3 times that of pentacene. For **7**, the 4,8-substituted derivative the reorganization energies obtained are much larger. On the other hand, with the substitutions the HOMO, LUMO, and the HLG can be varied which offers a wide scope of fine-tuning the property and also obtaining p-type or n-type semiconduction. Most of the molecules studied here pack in the solid state in an almost herringbone pattern to minimize the repulsions. The key parameter for transport in these molecules is seen to be the transfer integral. Here we obtain large transfer integrals between the HOMOs for the p-type semiconduction and for the n-type semiconduction large transfer integrals between the LUMOs. In fact, the largest value obtained is 193 meV in **2** for hole transport and the molecules perpendicular to that have also large transfer integral of 104 meV, indicating that at least in two orthogonal directions there is large hole transport. But the possibility of a 3-dimensional charge transfer is not seen. We conclude that these molecules with judicious substitution that can lead to a favorable packing can play a role in the development of OFETs.

ASSOCIATED CONTENT

Supporting Information

Molecular structures of **2**−**4** and **7** with bond numbering; comparison of optimized geometries with crystal geometries; theoretical estimation of VEA, AEA, and reorganization energies; changes in geometrical parameters; contributions of vibrations to the geometry relaxation; transfer integrals obtained using ESID method; uncorrected interaction energies along with counterpoise correction and frontier molecular orbitals of the dimers. This material is available free of charge via the Internet at http://pubs.acs.org.

AUTHOR INFORMATION

Corresponding Author

*E-mail: bhanu2505@yahoo.co.in.

Notes

The authors declare no competing financial interest.

ACKNOWLEDGMENTS

The authors thank the Director, IICT, and The Head, Inorganic and Physical Chemistry Division, IICT, for their constant encouragement in this work. N.L.J., B.P., and A.T. thank CSIR, India, for the JRF and SRF fellowships, respectively.

REFERENCES

(1) Tang, C. W.; Vanslyke, S. A. *Appl. Phys. Lett.* **1987**, *51*, 913−915.
(2) Slyke, S. A. V.; Chen, C. H.; Tang, C. W. *Appl. Phys. Lett.* **1996**, *69*, 2160−2162.
(3) Mas-Torrent, M.; Rovira, C. *Chem. Soc. Rev.* **2008**, *37*, 827−838.
(4) Shirota, Y.; Kageyama, H. *Chem. Rev.* **2007**, *107*, 953−1010.
(5) Garnier, F. *Chem. Phys.* **1998**, *227*, 253−262.

(6) Klauk, H. *Chem. Soc. Rev.* **2010**, *39*, 2643−2666.
(7) Lin, Y.; Li, Y.; Zhan, X. *Chem. Soc. Rev.* **2012**, *41*, 4245−4272.
(8) Hains, A. W.; Liang, Z. Q.; Woodhouse, M. A.; Gregg, B. A. *Chem. Rev.* **2010**, *110*, 6689−6735.
(9) O'Neill, M.; Kelly, S. M. *Adv. Mater.* **2011**, *23*, 566−584.
(10) Tobjork, D.; Osterbacka, R. *Adv. Mater.* **2011**, *23*, 1935−1961.
(11) Jung, B. J.; Tremblay, N. J.; Yeh, M.-L.; Katz, H. E. *Chem. Mater.* **2011**, *23*, 568−582.
(12) Wang, C.; Dong, H.; Hu, W.; Liu, Y.; Zhu, D. *Chem. Rev.* **2012**, *112*, 2208−2267.
(13) Li, J.; Wang, M.; Ren, S.; Gao, X.; Hong, W.; Li, H.; Zhu, D. *J. Mater. Chem.* **2012**, *22*, 10496−10500.
(14) Mitsui, C.; Soeda, J.; Miwa, K.; Tsuji, H.; Takeya, J.; Nakamura, E. *J. Am. Chem. Soc.* **2012**, *134*, 5448−5451.
(15) Qiao, Y.; Guo, Y.; Yu, C.; Zhang, F.; Xu, W.; Liu, Y.; Zhu, D. *J. Am. Chem. Soc.* **2012**, *134*, 4084−4087.
(16) Deng, P.; Yan, Y.; Wang, S.-D.; Zhang, Q. *Chem. Commun.* **2012**, *48*, 2591−2593.
(17) Yun, S. W.; Kim, J. H.; Shin, S.; Yang, H.; An, B.-K.; Yang, L.; Park, S. Y. *Adv. Mater.* **2012**, *24*, 911−915.
(18) Takimiya, K.; Shinamura, S.; Osaka, I.; Miyazaki, E. *Adv. Mater.* **2011**, *23*, 4347−4370.
(19) Mas-Torrent, M.; Rovira, C. *Chem. Rev.* **2011**, *111*, 4833−4856.
(20) Qiao, Y.; Wei, Z.; Risko, C.; Li, H.; Bredas, J.-L.; Xu, W.; Zhu, D. *J. Mater. Chem.* **2012**, *22*, 1313−1325.
(21) Otón, F.; Pfattner, R.; Pavlica, E.; Olivier, Y.; Moreno, E.; Puigdollers, J.; Bratina, G.; Cornil, J. r. m.; Fontrodona, X.; Mas-Torrent, M.; Veciana, J.; Rovira, C. *Chem. Mater.* **2011**, *23*, 851−861.
(22) Wang, L.; Zhang, H. *J. Phys. Chem. C* **2011**, *115*, 20674−20681.
(23) Coropceanu, V.; Cornil, J.; da Silva, D. A.; Olivier, Y.; Silbey, R.; Bredas, J. L. *Chem. Rev.* **2007**, *107*, 926−952.
(24) Koh, S. E.; Risko, C.; da Silva Filho, D. A.; Kwon, O.; Facchetti, A.; Brédas, J. L.; Marks, T. J.; Ratner, M. A. *Adv. Funct. Mater.* **2008**, *18*, 332−340.
(25) Delgado, M. C. R.; Kim, E. G.; da Silva, D. A.; Bredas, J. L. *J. Am. Chem. Soc.* **2010**, *132*, 3375−3387.
(26) Mondal, R.; Ko, S. W.; Bao, Z. N. *J. Mater. Chem.* **2010**, *20*, 10568−10576.
(27) Qian, G.; Wang, Z. Y. *Chem.—Asian J.* **2010**, *5*, 1006−1029.
(28) Kulkarni, A. P.; Tonzola, C. J.; Babel, A.; Jenekhe, S. A. *Chem. Mater.* **2004**, *16*, 4556−4573.
(29) Anthony, J. E.; Facchetti, A.; Heeney, M.; Marder, S. R.; Zhan, X. *Adv. Mater.* **2010**, *22*, 3876−3892.
(30) Cornil, J.; Brédas, J. L.; Zaumseil, J.; Sirringhaus, H. *Adv. Mater.* **2007**, *19*, 1791−1799.
(31) Liu, Y.-Y.; Song, C.-L.; Zeng, W.-J.; Zhou, K.-G.; Shi, Z.-F.; Ma, C.-B.; Yang, F.; Zhang, H.-L.; Gong, X. *J. Am. Chem. Soc.* **2010**, *132*, 16349−16351.
(32) Wu, W.; Liu, Y.; Zhu, D. *Chem. Soc. Rev.* **2010**, *39*, 1489−1502.
(33) lack, H. T.; Liu, S.; Sheares Ashby, V. *Org. Lett.* **2011**, *13*, 6492−6495.
(34) Mike, J. F.; Inteman, J. J.; Ellern, A.; Jeffries-El, M. *J. Org. Chem.* **2010**, *75*, 495−497.
(35) Pang, H.; Vilela, F.; Skabara, P. J.; McDouall, J. J. W.; Crouch, D. J.; Anthopoulos, T. D.; Bradley, D. D. C.; De Leeuw, D. M.; Horton, P. N.; Hursthouse, M. B. *Adv. Mater.* **2007**, *19*, 4438−4438.
(36) McEntee, G. J.; Vilela, F.; Skabara, P. J.; Anthopoulos, T. D.; Labram, J. G.; Tierney, S.; Harrington, R. W.; Clegg, W. *J. Mater. Chem.* **2011**, *21*, 2091−2097.
(37) Mamada, M.; Nishida, J.; Tokito, S.; Yamashita, Y. *Chem. Lett.* **2008**, *37*, 766−767.
(38) Kang, J. G.; Kim, H. J.; Jeong, Y. K.; Nah, M. K.; Park, C.; Bae, Y. J.; Lee, S. W.; Kim, I. T. *J. Phys. Chem. B* **2010**, *114*, 3791−3798.
(39) Frisch, M. J.; Trucks, G. W.; Schlegel, H. B.; Scuseria, G. E.; Robb, M. A.; Cheeseman, J. R.; Scalmani, G.; Barone, V.;Mennucci, B.; Petersson, G. A.; et al. *Gaussian 09, Revision B.01*; Gaussian, Inc.: Wallingford, CT, 2010.
(40) Becke, A. D. *J. Chem. Phys.* **1993**, *98*, 5648−5652.
(41) Becke, A. D. *J. Chem. Phys.* **1996**, *104*, 1040−1046.
(42) Lee, C. T.; Yang, W. T.; Parr, R. G. *Phys. Rev. B* **1988**, *37*, 785789.
(43) Kim, D.; Salman, S.; Coropceanu, V.; Salomon, E.; Padmaperuma, A. B.; Sapochak, L. S.; Kahn, A.; Bredas, J. L. *Chem. Mater.* **2010**, *22*, 247−254.
(44) Brédas, J. L.; Calbert, J. P.; da Silva Filho, D. A.; Cornil, J. *Proc. Natl. Acad. Sci. US.A.* **2002**, *99*, 5804−5809.
(45) Cheng, Y. C.; Silbey, R. J.; da Silva, D. A.; Calbert, J. P.; Cornil, J.; Bredas, J. L. *J. Chem. Phys.* **2003**, *118*, 3764−3774.
(46) Wang, L.; Nan, G.; Yang, X.; Peng, Q.; Li, Q.; Shuai, Z. *Chem. Soc. Rev.* **2010**, *39*, 423−434.
(47) Shuai, Z. G.; Wang, L. J.; Li, Q. K. *Adv. Mater.* **2011**, *23*, 1145−1153.
(48) Marcus, R. A. *J. Chem. Phys.* **1956**, *24*, 966−978.
(49) Li, C.-H.; Huang, C.-H.; Kuo, M.-Y. *Phys. Chem. Chem. Phys.* **2011**, *13*, 11148−11155.
(50) Reimers, J. R. *J. Chem. Phys.* **2001**, *115*, 9103−9109.
(51) Grozema, F. C.; Siebbeles, L. D. A. *Int. Rev. Phys. Chem.* **2008**, *27*, 87−138.
(52) Valeev, E. F.; Coropceanu, V.; da Silva, D. A.; Salman, S.; Bredas, J. L. *J. Am. Chem. Soc.* **2006**, *128*, 9882−9886.
(53) You, Z.-Q.; Shao, Y.; Hsu, C.-P. *Chem. Phys. Lett.* **2004**, *390*, 116−123.
(54) Ohta, K.; Closs, G. L.; Morokuma, K.; Green, N. J. *J. Am. Chem. Soc.* **1986**, *108*, 1319−1320.
(55) Farazdel, A.; Dupuis, M.; Clementi, E.; Aviram, A. *J. Am. Chem. Soc.* **1990**, *112*, 4206−4214.
(56) Lu, S.-Z.; Li, X.-Y.; Liu, J.-F. *J. Phys. Chem. A* **2004**, *108*, 4125−4131.
(57) Li, X.-Y.; He, F.-C. *J. Comput. Chem.* **1999**, *20*, 597−603.
(58) Zhao, Y.; Truhlar, D. *Theor. Chem. Acc.* **2008**, *120*, 215−241.
(59) Grimme, S. *J. Comput. Chem.* **2006**, *27*, 1787−1799.
(60) Grimme, S. *J. Chem. Phys.* **2006**, *124*, 034108−034116.
(61) Schwabe, T.; Grimme, S. *Phys. Chem. Chem. Phys.* **2007**, *9*, 3397−3406.
(62) Jansen, H. B.; Rose, P. *Chem. Phys. Lett.* **1969**, *3*, 140−143.
(63) Boys, S. F.; Bernardi, F. *Mol. Phys.* **1970**, *19*, 553−566.
(64) Mück -lichtenfeld, C.; Grimme, S.. *Mol. Phys.* **2007**, *105*, 2793−2798.
(65) Giannozzi, P.; Baroni, S.; Bonini, N.; Calandra, M.; Car, R.; Cavazzoni, C.; Ceresoli, D.; Chiarotti, G. L.; Cococcioni, M.; Dabo, I.; et al. *J. Phys.: Condens. Matter* **2009**, *21*, 395502. (Also available via the Internet at http://www.quantum-espresso.org.)
(66) Perdew, J. P.; Burke, K.; Ernzerhof, M. *Phys. Rev. Lett.* **1996**, *77*, 3865−3868.
(67) Chen, H.-Y.; Chao, I. *Chem. Phys. Lett.* **2005**, *401*, 539−545.
(68) Adamo, C.; Barone, V. *J. Chem. Phys.* **1999**, *110*, 6158−6170.
(69) Dovesi, R.; Orlando, R.; Civalleri, B.; Roetti, C.; Saunders, V. R.; Zicovich-Wilson, C. M. Z. *Kristallogr.* **2005**, *220*, 571.
(70) Dovesi, R.; Saunders, V. R.; Roetti, C.; Orlando, R.; Zicovich-Wilson, C. M.; Pascale, F.; Civalleri, B.; Doll, K.; Harrison, N. M.; Bush, I. J.; D'Arco, P.; Llunell, M.; *CRYSTAL09 Users' Manual*; University of Torino: Torino, Italy, 2009.